

Measuring proton energies and fluxes using EIT (SOHO) CCD areas outside the solar disk images

L.V. DIDKOVSKY,¹ D.L. JUDGE,¹ A.R. JONES,¹ E.J. RHODES, JR.,¹ AND J.B. GURMAN,²

¹ University of Southern California, 835 W. 37th Street, SHS, Los Angeles, California 90089-1341, USA

² NASA Goddard Space Flight Center, Greenbelt, Maryland 20771, USA

Received <date>; accepted <date>; published online <date>

Abstract. An indirect proton flux measuring tool based on discrimination of the energy deposited by protons in 128×128 pixel EIT CCD areas outside the solar disk images is presented. Single pixel intensity events are converted into proton incident energy flux using modeled energy deposition curves for angles of incidence ± 60 deg in four EIT spatial areas with different proton stopping power. The extracted proton flux is corrected for both the loss of one-pixel events in the range of angles of incidence as well as for the contribution to the single pixel events resulting from scattered middle-energy protons (low-energy or high-energy particles are stopped by the EIT components or pass through them, accordingly). A simple geometrical approach was found and applied to correct for a non-unique relation between the proton-associated CCD output signal and the incident proton energy. With this geometrical approximation four unique proton incident energy ranges were determined as 45–49, 145–154, 297–335, and 390–440 MeV. The indirect proton flux measuring tool has been tested by comparing Solar Energetic Particles (SEP) flux temporal profiles extracted from the EIT CCD frames and downloaded from the GOES database for the Bastille Day (BD) of 2000 July 14 and the more recent 2005 January 20 events. The SEP flux temporal profiles and proton spectra extracted from the EIT in the relatively narrow energy ranges between 45 and 440 MeV reported here are consistent with the related GOES profiles. The four additional EIT extracted ranges provide higher energy resolution of the SEP data.

Key words: Solar Energetic Particles, Solar flare events, Proton flux, Proton spectra, Space Weather

©0000 WILEY-VCH Verlag GmbH & Co. KGaA, Weinheim

1. Introduction

Major solar flares observed in X-ray and Extreme Ultraviolet (EUV) radiation allow building and comparing both flare dynamics for the impulsive phases of flares and their impact on the Earth's ionosphere, e.g. (Tsurutani et al. 2005). Study of SEP events produced by those flares, and accelerated by interplanetary shock formations associated with Coronal Mass Ejections (CMEs), may clarify the relations between flare (and CME) characteristics, and the spectra of post-flare events.

If the particle flux spectra have different ‘fingerprints’ for different flares, then it would be possible to transfer these differences seen at 1 AU (or, better, seen from a few different distances to the Sun, (Lin 2005)), and to combine the SEP flux measurements with corresponding X-ray and EUV flux measurements for creating a flare's energy spectrum and clarifying the acceleration mechanism. This task would require both the time-dependent and distance-dependent particle flux

spectra in a number of energy ranges and an appropriate time-dependent model of particle acceleration and propagation, e.g. (Tsurutani et al. 2003), as well as high-cadence measurements in X-ray and EUV bands for the impulsive phase of the flare. As an initial phase of this kind of study we would like to start with a number of relatively narrow energy bands extracted from the SOHO/EIT dark CCD corner areas in addition to the existing broadband GOES proton flux data.

Particle flux spectra in high-energy ranges may reveal another side in an analysis of CMEs and SEP (Gopalswamy et al. 2004). The authors found that “the active region area has no relation with both the SEP intensity and CME speed, thus supporting the importance of CME interaction”. Is there any relation between a flare intensity (class) and SEP proton spectra?

High-energy particles create a “noise” background in a solid state detector, e.g. (Williams, Arens & Lanzerotti 1968), strongly affecting any space-based electronics (Adams, Tsao & Silberberg 1981). The worst case scenario occurs when the detector consists of a small number of relatively large pixels.

The result of photon measurements in this case is strongly contaminated by proton-created electron-hole pairs.

Our goal in this work was to find a way of converting the proton noise background into a useful signal and to study SEP events in narrower ranges of energies than available from the NOAA GOES proton measurements.

SOHO/EIT (Delaboudiniere et al. 1996) uses a 1024×1024 thinned, back-illuminated CCD. Scattered protons usually hit different pixels, depositing either all or a part of their energy in the CCD active silicon layer, allowing analysis of the density of the affected pixels and the energy of the detected protons as in the analysis of a stellar field. To measure the energy of the proton, some relations between incident proton energy in the range of the angles of incidence, and the pixel's resulting intensity, are required. The presence of some optical and mechanical components through which the detected protons must pass requires that the stopping power of those components be modeled.

2. Data observation and the measuring tool

A few sets of 1024×1024 EIT EUV solar images in the 19.5 nm spectral window were used to extract the proton events. Each set covers the period of the impulsive phase of the flare and some pre-flare and post-flare stages. A summary of the data used is given in Table 1.

Table 1. EIT 19.5 nm data observations.

| Date | Images | Cadence (min) |
|-------------|--------|---------------|
| 2000 Jul 14 | 91 | 15.6 |
| 2000 Jul 15 | 71 | 19.9 |
| 2005 Jan 20 | 93 | 15.2 |

The information about proton events was extracted from two (N-W and S-W) corner areas of the CCD images (see subsection 5.1 and Figure 6), each of 128×128 pixels in size. These areas are outside of centered solar images but consist of some bright coronal features visible in the EUV, and some instrumental sources of noise, like a bright unfocussed grid associated with the filter support mesh structure, which develops during an impulsive phase of a solar flare. To reduce the contamination of the proton-related signals by these features, a spatial filtering (result = original data minus filter) was applied to each image of the series after subtracting dark frames. The size of the filter's window was selected as minimal as possible, 3 pixels, to effectively filter out all low spatial frequencies of the unwanted background.

2.1. One-pixel SEP events

Clearly, the only correct interpretation of the pixel-based intensity detector signal is when the relation "one particle - one pixel" is used. In the other two cases when either one particle hits two (or more) pixels or two (or more) particles deposit energy in the same pixel, the energy deposited in the CCD

pixel is shared between those events in some unknown proportion, making the planar CCD an inappropriate detector.

The first of these two cases may be easily detected and eliminated using an appropriate data reduction algorithm. The algorithm we developed is specifically designed to filter out all but single-pixel events.

The second case may be considered unimportant too in our analysis of relatively small fluxes, collecting times, and the size of the pixels. For any analyzed range of SEP energy the rate of one-pixel events, registered during the EIT collecting time, is not larger than 0.5 percent, and is substantially smaller for high-energy ranges. The statistical error introduced by the "two particles - one pixel" events is less than the detecting sensitivity of this method, about 0.013 particles/cm²/s/sr/MeV. This means that the EIT CCD detector can be used to analyze the energies of an incident particle quasi-isotropic distribution.

The EIT CCD geometry (21 μm square pixels with the thickness of the active silicon layer $d=12 \mu\text{m}$) (Moses 2004) determines the opening of both front and back-side cones for incoming particles to create the one-pixel events. The axis of the cones coincides with the EIT optical axis and have a maximal opening of ± 68 deg. Only about 10⁻³ % or less of all quasi-isotropic particles could still hit a pixel in its corner points and produce the one-pixel event. For a simplified case of this calculation with axial symmetry and a cylindrical pixel ($D = 21 \mu\text{m}$) the maximal opening is about ± 60.25 deg. We have limited the outer edge of the opening to ± 60 deg with the amount of the one-pixel events at this edge of about 1.5 %. In contrast with this, about 100 % of all particles of the quasi-isotropic flux could produce the one-pixel events at normal incidence.

Obviously, any particles whose trajectory is inclined with respect to a normal incidence path has a probability to create two or more pixel events. This probability for the micro-isotropic fluence (isotropic over the size of the area of detectors used) is directly related to the CCD geometry and is a linear function of the angle of incidence with probability $P(0 \text{ deg})=0$ and $P(60 \text{ deg})=0.985$. It was used to correct the underestimated one-pixel SEP flux events over the two-pixel events for any inclined particle path, see k_1 in the Equation (2).

2.2. Four spatial areas of the EIT

In the range of incident proton trajectories which create one-pixel events (± 60 deg) we have determined four spatial areas with either different opto-mechanical EIT components and substantially different stopping power or with a large range of the angles of incidence. Each of the four areas requires a separate model of the proton energy deposition relations. These relations may be represented either by a unique curve with very small deviations on the ranges of the area or by two distinctive curves corresponding to the edges of the area and showing a wider range of energy deposition relations. These areas are (Figure 1): (i) an angular opening ± 2 deg through the secondary mirror and some mechanical components; (ii) a space between the secondary (SM) and primary mirror (PM)

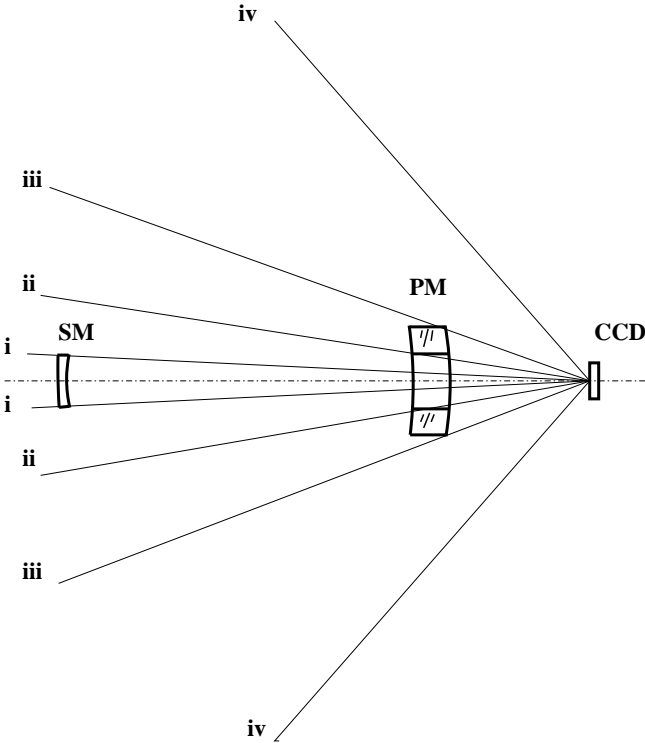


Fig. 1. A simplified schematic view of the EIT (not to scale) and chosen four spatial area edges i-i, ii-ii, iii-iii, and iv-iv with different conditions in these areas for deposition of proton energy to the CCD pixels.

with opening $\pm 2 - 8$ deg through the hole in the PM; (iii) the space through the PM with opening of $\pm 8 - 18$ deg; and (iv) the space between the outer diameter of the PM and the chosen outer edge of the one-pixel event openings, $\pm 18 - 60$ deg.

Five curves for determining proton deposited energy (PDE) in the CCD at incidence angles 0, 5, 13, 18, and 60 deg and three curves for proton stopping power (PSP) at 0, 8, and 18 deg were modeled. The PSP for the area ii-iii (through the PM) was modeled by two curves to determine changes of the stopping power associated with the changes of the angle of incidence between 8 and 18 deg. The calculated PSP were used to make a corresponding correction to the proton incident energy when the relations of the energy deposited in the CCD versus the angle of incidence were finally modeled. For the three central areas with the opening of $\pm 0 - 18$ deg we have assumed determining PDE for the middle angles of these area angular ranges only, because changing of the angle of incidence from 0 deg (first area, center) to 18 deg (third area, outer edge) just slightly changes the effective length of the mean path through the CCD silicon layer of $0.6 \mu\text{m}$, which makes corresponding curves practically overlapped. For the area (iii - iv) we calculated PDE for both edges of its opening to have a corresponding range of PDE.

For the same cone openings from the back side of the EIT (the spacecraft side) we have assumed that the quite thick CCD housing and spacecraft components represent a substantial stopping power for the proton flux, which is directed backward, to the Sun. This stopping power is sufficient to

stop protons with lower energies or substantially shift their incident energy to a lower energy range. The typical proton spectra in the MeV energy ranges (e.g. GOES data) show a substantial decrease of the proton flux when the energy is changed from a lower to a higher level. It means that high-energy protons that could still come through the back side of the EIT would add to the normally intense low-energy flux detected from the front side of the EIT, but no more than a small fraction (1-2 %) or less of the “weakened” high-energy protons. If this assumption is correct, the SEP flux in the low-energy bands should be slightly higher than the one measured by dedicated instruments. This error should be maximal (a few percent) during the short initial time of the SEP flux event, corresponding to the high-energy proton flux peak. Moreover, because the arriving time is different (higher-energy particles arrive earlier than low-energy ones), this error related to the back-side particles could create a peak in the low-energy temporal SEP flux profile a while before the pure low-energy peak. The SEP proton fluxes extracted from the EIT show (see section 3) that the assumption to ignore the back-side particles is correct within the error of about 1-2 %.

Modeling of energy deposited by protons in the CCD active silicon layer was based on the Stopping and Range of Ions in Matter program (SRIM) (Ziegler & Biersack 2003). Both PSP and PDE were calculated with the Monte-Carlo statistics for 5000 protons each. As the SRIM material library does not contain the zerodur glass ceramic $\rho = 2.53 \text{ g/cm}^3$ used for producing the EIT mirrors, the closest appropriate optical material - quartz $\rho = 2.32 \text{ g/cm}^3$ and silicon $\rho = 2.32 \text{ g/cm}^3$ (for a reference) were used for modeling the stopping power with practically the same result. The EIT envelope with thickness of about 75 mils (1.9 mm) (Newmark 2005) of aluminum was considered with variable thickness as a function of the angle of incidence. The energy deposited by recoils in the silicon layer was ignored as it was a few orders of magnitude less than that deposited directly by ions. Figure 2 shows the modeled energy deposition curves (converted into DNs) for the four spatial areas of the EIT (Fig 1), where area 1 is i-i, area 2 is i-ii, area 3 is ii-iii, and area 4 is iii-iv.

Energy deposited in the CCD E_d (not shown in Figure 2) was converted into the CCD camera output signal (DN) using the following relation.

$$DN_i = E_{d,i}/E_p/CCD_s \quad (1)$$

where E_p is the deposited energy required to create an electron-hole pair, $E_p = 3.65 \text{ eV}$; CCD_s is the sensitivity of the CCD camera, $CCD_s = 18 \text{ e}/DN$; i is the spatial area index.

The CCD sensitivity CCD_s (Delaboudiniere et al. 1996) corresponds to the $18 \text{ e}/DN$ measured at the launch time. We have assumed that even if the CCD sensitivity has changed due to solar EUV radiation of the illuminated solar disk pixels, the corner (dark) area pixels used for this analysis should all have about the same pre-launched sensitivity.

Figure 2 shows that the whole range of proton incident energies has two distinctive sub-ranges, namely between 40 and 180 MeV and between 180 and 460 MeV. The difference between these two sub-ranges is reflected by the different CCD

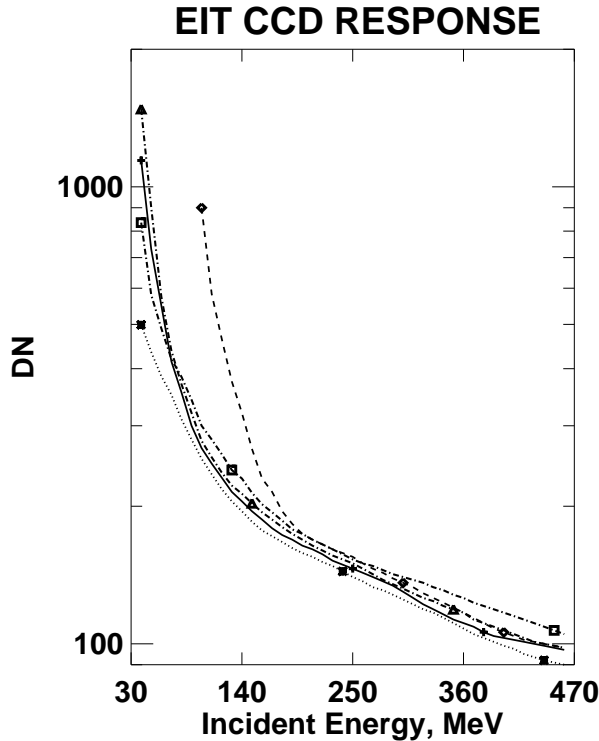


Fig. 2. EIT CCD camera Discrete Numbers (DN) as a function of proton incident energy for the four EIT opening areas (Fig 1) marked with pluses (solid line for area 1), asterisks (dotted for area 2), diamonds (dashed for area 3), triangles and squares (dash-dotted lines for area 4 at 18 deg and 60 deg, correspondingly).

response of the two sub-ranges. In the first sub-range both the stopping power in each of the four spatial areas and different angles of incidence strongly affect the amount of energy deposited due to the high level of interactions between the low-energy protons and the active silicon layer. The influence of these two factors in the second sub-range is relatively small, because high-energy protons transit the silicon layer with a lower level of interactions. Figure 2 also shows that the first sub-range has two distinctive portions, 40–110 and 110–180 MeV. The lowest energy portion represents protons penetrating through EIT components in all areas, except the area through the PM. The EIT PM together with the EIT envelope can stop all protons if their energy is below 110 MeV and angles of incidence are ± 8 –18 deg.

Because of the wide area of the energy deposition curves, one can see that the CCD response with DN equal to, e.g., 490 may be created by protons with energies between 42 MeV (area i–ii) and 120 MeV (area ii–iii). The real difficulty of any direct approach to convert the DNs into proton incident energies could come from the fact that protons with any exact energy in the range of 42–120 MeV, determined above, might produce a wide range of DNs as a function of the angle of incidence (the spatial area). For example, protons with the incident energy of 115 MeV (a vertical line at 115 MeV) would have the response from 240 to 690 DNs. This means that the direct method of converting proton incident energy

into the CCD output signal (Figure 2) has no unique solution, thus producing the signal contamination. To solve this problem a simple geometrical approach has been found. It is described in the next subsection.

2.3. Incident SEP energy ranges and corresponding DNs

Figure 2 shows that the task of extracting the information about the incident proton energy flux from the CCD intensity signal is not a trivial one. A vertical line, which corresponds to a given incident proton energy on Fig 2 intersects a number of energy deposition curves and shows a corresponding range of DNs, making the task of interpretation of the results of measurements clearly uncertain. Nevertheless, in an approximation of a geometrical approach, shown in Figure 3, this task can be solved.

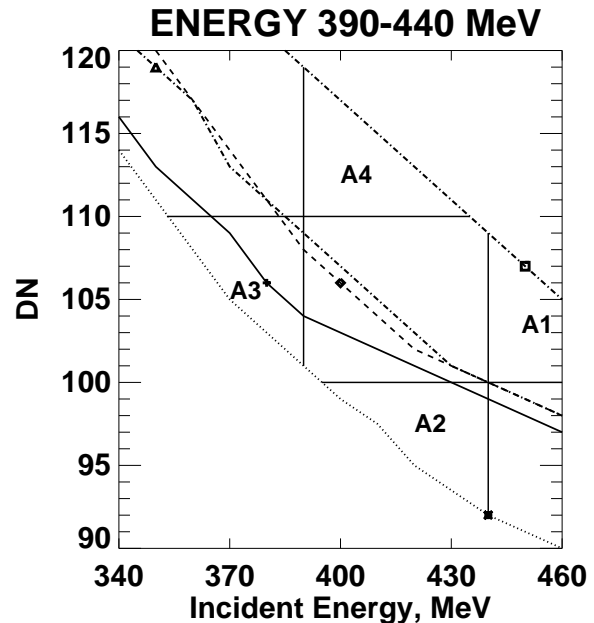


Fig. 3. An enlarged fragment of Fig 2 used for determination of the highest energy range (see Table 2). The determined energy range between two vertical lines at 390 and 440 MeV leads to a minimal signal contamination if combined with the appropriate signal range between two horizontal lines at $DN_1 = 100$ and $DN_2 = 110$. The condition to totally avoid the signal contamination is to make areas A1 and A2 as well as A3 and A4 equal to each other. The triangle shaped areas A1–A4 are created by two marginal energy deposition curves (marked with asterisk and square) and crossed straight lines.

Figure 3 shows a portion of the energy deposition area (high-energy part of Fig 2) between two marginal energy deposition curves marked with an asterisk (dotted line for area 2) and a square (dash-dotted line for area 4 at 60 deg). A combination of two horizontal lines with two vertical lines shows the condition when two of the four triangle shaped areas A1 and A3 may be virtually transferred, replacing other two areas A2 and A4 if the areas A1 and A2, as well as A3 and A4, are equal to each other. The virtual transferring works

when, e.g., the area A1, which adds to the CCD signal between $DN_1 = 100$ and $DN_2 = 110$ but should not add in the $E_1 = 390$ MeV through $E_2 = 440$ MeV energy range, is equal to A2, which does not add to the CCD signal between DN_1 and DN_2 but should be counted in the E_1 – E_2 energy range. With the virtual transfer, when the A1 (A3) area “replaces” the A2 (A4), the appropriate range of DNs between DN_1 and DN_2 corresponds to the incident energy range from E_1 to E_2 .

As an example of using the geometrical approach we have determined four incident proton energy ranges and corresponding four ranges of DNs (Table 2). The number of determined energy bands may be larger than the four we have used in this analysis if they are consistent with the requirement of the geometrical approach found.

Table 2. Deposited energies E_d and DNs for incident energy subranges E_i .

| E_{1-2} (MeV) | Median E_i (MeV) | ΔE_i (MeV) | E_d (keV) | DN_i |
|--------------------|-----------------------|-----------------------|----------------|----------|
| 45–49 | 47 | 4 | 85.4–62.4 | 1300–950 |
| 145–154 | 150 | 9 | 15.2–14.8 | 232–225 |
| 297–335 | 316 | 38 | 8.9–8.2 | 135–125 |
| 390–440 | 415 | 50 | 7.2–6.6 | 110–100 |

2.4. High-energy SEP fluxes

The proton flux temporal profiles for any of the four energy subranges E_i were found as:

$$F_i(E_i, t) = k_1 * N_i(E_i, t) / S / T / \Delta E_i / \alpha - k_2 \quad (2)$$

$N_i(E_i, t)$ is a mean sum of pixels in a given subrange of Discrete Numbers DN_i :

$$N_i(E_i, t) = 0.5 \sum_{DN_i} P_{1,i} + P_{2,i} \quad (3)$$

where $k_1 = 2$, a statistical coefficient to cover the loss of the one-pixel events underestimated due to converting them into two-pixel events at the angles of incidence larger than 0.0 deg; S is the area of 128 × 128 pixels, $S = 0.0723 \text{ cm}^2$; T is the mean integration time (12.6 s), which includes the camera exposure time plus shutter operation time (shutter is transparent to high energy protons); ΔE_i is a number of MeV for a given energy subrange; $\alpha = 0.84 \text{ sr}$ corresponds to the cone opening of ± 30 deg. This opening was determined as statistically equivalent to the whole opening of ± 60 deg if the probability for both one-pixel and two-pixel events in this smaller area could be constant and equal to 1.0 (equal to zero outside of this area), instead of real uniform (linear) distribution of probabilities from 1.0 to 0.015 and from 0.0 to 0.985 for one-pixel and two-pixel events at 0 and 60 deg, accordingly; DN_i is the range of DNs corresponding to the contamination-free range of E_i , (Table 2); P_{1-2i} are corresponding numbers of proton-pixels events in two S-areas for the energy subrange E_i ; k_2 is a statistical coefficient to correct the flux over produced by scattered on the EIT mechanical components particles initially coming outside the one-pixel opening. This coefficient depends of the intensity of the SEP flux and is 0.4 for

the BD and 2005 January 20 events. The approximate relation we inferred to determine this coefficient for intense SEP flux events is

$$k_2 = \ln (4 \sqrt{F_{80-165}}) \quad (4)$$

where $F_{80-165} \geq 1.0$ is GOES maximal SEP event flux in the energy range of 80–165 MeV.

3. Temporal EIT and GOES SEP flux profiles

The EIT-based SEP flux measuring tool was tested with two geo-effective solar flare events (Table 1) and compared to the available GOES database temporal profiles taken in different and lower resolution energy ranges. The GOES energy ranges used for comparison are 40, 80–165, and 165–500 MeV. The results of the calculation of proton fluxes for the analyzed flare events are shown in Figure 4.

Because of the quite small size of the corner CCD areas, each of 128 × 128 pixels, which is equivalent to 0.072 cm^2 area, the lower value for SEP fluxes in Figure 4 is limited for both EIT extracted fluxes as well as the GOES fluxes, to 0.003 particles/ $\text{cm}^2/\text{s}/\text{sr}/\text{MeV}$, which is four times lower than the sensitivity of the EIT proton flux measuring tool (0.013 particles/ $\text{cm}^2/\text{s}/\text{sr}/\text{MeV}$). This limit allows some pre-flare details of the GOES flux to be seen.

GOES data (GOES-8 for 2000/07/14 and GOES-11 for the 2005/01/20 event) were over-plotted on Figure 4 with thin lines for a reference. Even with different energy band resolution one can see that both EIT and GOES temporal profiles show a good match in both the flux maximal values and the temporal profiles. Some differences in the level of measured SEP flux are consistent with the known decrease of the flux toward the high-energy ranges. Specifically, extracted EIT SEP flux, e.g., for the 45–49 MeV energy range (mean is 47 MeV) is lower than that measured by GOES for 40 MeV SEP. Some fast changes in the EIT SEP flux temporal profiles are lost due to the 13–20 min image cadence, compared to the 1 min cadence in the GOES data.

Temporal EIT and GOES flux profiles in the high-energy ranges show more differences than one can see between the 47 and 40 MeV profiles. When the number of proton pixel-events registered by the EIT CCD drops to a few as the high-energy flux decreases, the EIT temporal profiles show fluctuations to the zero flux level. The important detail is that when the flux value resumes, it corresponds to the whole energy range’s trend.

Figure 4 has over-plotted GOES X-ray (0.1–0.8 nm) temporal profiles to show the time delays between the X-ray peak of the solar flare and corresponding SEP flux peaks. These time delays may be used to study relativistic features of some post-flare SEP events with a larger number of energy ranges than is available from the GOES database.

4. EIT and GOES proton flux spectra

An important detail of the current work is to show that even four additional, but narrower, EIT energy ranges substantially

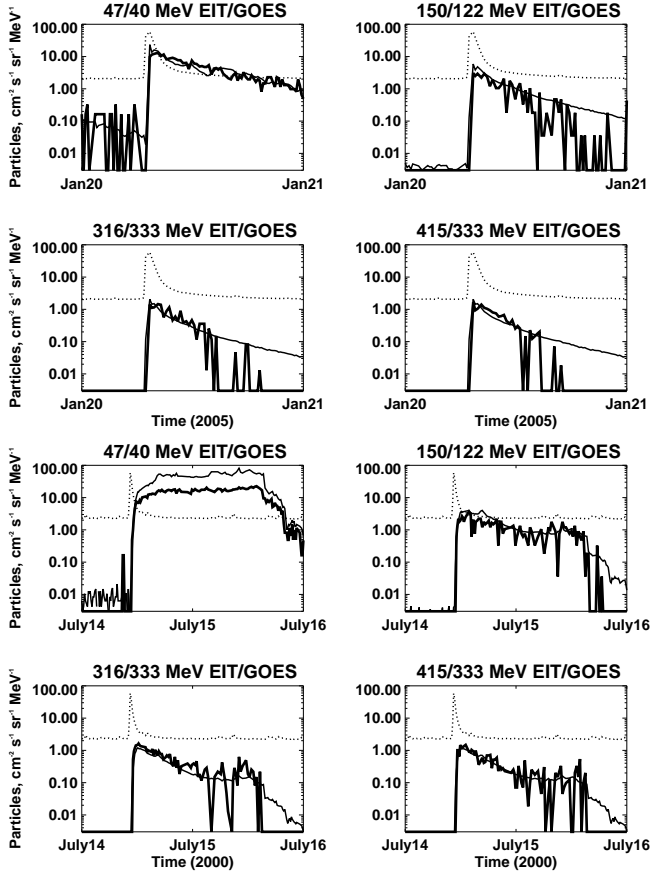


Fig. 4. Proton fluxes (particles, $1/\text{cm}^2/\text{s}/\text{sr}/\text{MeV}$) extracted from EIT (thick line) and from GOES database (thin line) for 2005 January 20 and 2000 July 14 events. The dotted line shows GOES X-ray data in arbitrarily units with 1-min cadence.

reduce the uncertainty of the “flux vs energy” proton spectra built with available GOES measurements. Figure 5 shows GOES and EIT proton spectra.

Proton spectra for both GOES and EIT data are in good agreement with each other. The GOES maximal flux values in the energy ranges 165–500 MeV for the analyzed events shown in Figure 5 as long bars are updated by higher resolution (shorter) EIT bars. The EIT bars make it possible to determine slopes of the proton spectra in the energy range of 145–440 MeV, which is not possible with the GOES long horizontal bars. The statistics for two analyzed events is quite small when attempting to develop some common slope characteristics for solar flare events. Nevertheless, an interesting feature of Figure 5 is that the “biggest proton event since 1989” after the X-7 solar flare of 2005 January 20 in the NOAA 10720 AR shows a substantially smaller total decrement than the one for the BD event with about the same slope in the high-energy range.

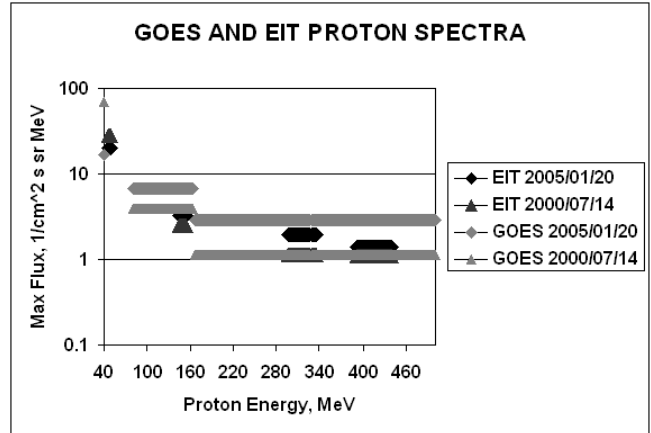


Fig. 5. GOES and EIT proton spectra for the 2000/07/14 and 2005/01/20 SEP events. The length of the horizontal bars reflects the energy range.

5. Discussion

5.1. Instrumental issues

Proton flux temporal profiles extracted from EIT and compared to the GOES-based profiles show good matching of time-variable changes for lower energy ranges. Higher energy flux profiles are more affected by some small additional flux due to scattering particles coming from the outside of the one-pixel opening. The number of scattered particles is directly related to the intensity of SEP flux event in the middle range of energies, e.g., GOES 80–165 MeV energy range (4). Lower and higher energy particles do not affect the measurements because they are either absorbed or go through the EIT components. The correction of the SEP flux by subtracting the “scattered” portion estimated as k_2 (4) develops itself mostly for the low-intense post-flare portions of the SEP flux temporal profiles not analyzed in this work.

Another feature of the EIT measuring tool is some spatial asymmetry in the one-pixel opening cone of ± 60 deg. Four 128×128 pixel corner CCD areas show two quite different pairs of the extracted proton flux signals. The signals extracted from the first pair, which consists of NW and SW pixel areas are in good agreement to each other and to the modeled energy deposition relations. The temporal flux profiles extracted from the second pair of the CCD pixel areas (NE and SE) are substantially different. They show some lower incident energy range than that correspondent to the range of DNs. This shift of the energy range may be caused by some spatial asymmetry of the EIT regarding its optical axis in the range of the one-pixel events opening of ± 60 deg. The most likely the difference is caused by the stopping power of other SOHO instruments. We have estimated this asymmetry comparing SEP flux temporal profiles for each of the four corner areas of the CCD. The extracted flux profiles from two of the four CCD areas, which correspond to the modeled energy deposition curves, were used for our analysis of the SEP events. The flux signal from other two CCD areas does not correspond to the modeled deposition energy curves and was excluded from the analysis. Figure 6 shows for 2000

January 20 event flux profiles marked with the thick line for the western CCD areas (calibrated and used), and with the thin line for the eastern CCD areas (we did not calibrate and use them).

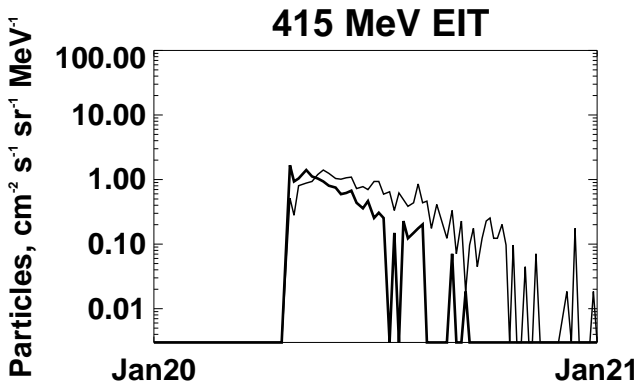


Fig. 6. Proton flux temporal profiles for 2005 January 20 event. The mean extracted from the EIT flux for the two western corner areas (thick line) is compared with the flux from the two eastern areas (thin line) in the energy range of 390–440 MeV.

The thin line (Figure 6) shows slower rise, a delayed maximum, larger flux, and smaller decrement, all typical features of a lower energy flux.

5.2. Temporal SEP flux profiles and proton spectra

The proton fluxes taken indirectly from EIT images in the four energy ranges of 45–49, 145–154, 297–335, and 390–440 MeV (Figure 4) were used to build proton spectra. All these spectra required extracting proton flux peak-values determined well above the lower limit of sensitivity of the EIT proton flux measuring tool, where the temporal profiles match corresponding GOES profiles and the statistical confidence is high.

Proton spectra showed two distinctive energy ranges clearly seen in the Figure 5, where fluxes extracted in EIT narrower energy ranges and compared to the GOES allowed seeing details of the high-energy spectra. Proton spectra in the high-energy range of 145–440 MeV show that the slopes for the two analyzed SEP events are quite small and similar. Lower energy range data for particles between 40 and 145 MeV demonstrates different trends for the analyzed events but this result should be verified with analysis of a larger number of SEP events.

If the lower energy proton spectra demonstrate different slopes, it may reveal either a flare specific or CME specific source of acceleration.

6. Conclusions

A proton flux measuring tool based on using a planar CCD detector was proposed, realized, and tested by comparing

proton flux temporal profiles and proton spectra extracted from the EIT with those taken from the GOES database. Temporal profiles (fluxes, shapes, and decrements) in the energy ranges of 45–49, 145–154, 297–335, and 390–440 MeV extracted from EIT correspond to or match available profiles from the NOAA GOES database in the energy ranges of 40, 80–165, and 165–500 MeV. Combined EIT-GOES proton spectra show much more detail when the GOES low energy resolution data are updated with the corresponding extracted EIT data in narrower energy ranges.

Proton spectra extracted from EIT for the analyzed SEP events show two distinctive energy regions, high- and low-energy, with different spectral features. The slopes of the proton spectra in the high-energy region (145–440 MeV) are quite small and similar to each other. In the lower energy range, between 40 and 145 MeV, slopes are substantially different for each analyzed event. If confirmed by a larger statistics, similar slopes of the proton flux spectra for the events with different energy releases may be strong evidence that the high-energy proton distribution does not depend on a flare class but follows a similar acceleration law, e.g., produced by a common post-flare acceleration (propagation) topology related to CME shock waves. Different slopes for the low-energy region may be related to either a flare specific or CME specific source of acceleration.

Acknowledgements. SOHO is a project of international cooperation between ESA and NASA. The Authors would like to thank Dan Moses and Frederic Auchere for some details of the EIT design. We are also grateful to Sasha Kosovichev and Linton Floyd for their comments and suggestions.

References

- Adams, J.H., Tsao, C.H. and Silberberg, R.: 1981, 'Cosmic Ray Effects on Electronics, Part I: The Near-Earth Particle Environment', *NRL Report*, **4506**.
- Delaboudiniere, J.P., Artzner, G.E., Brunaud, J. et al.: 1996, 'EIT: Extreme-Ultraviolet Imaging Telescope for the SOHO Mission', *Solar Physics* **162**, p. 291.
- Gopalswamy, N., Yashiro, S., Krucker, S., and Howard, R.A.: 2004, 'CME Interaction and the Intensity of Solar Energetic Particle Events', *In Proc. of IAU Symp. No. 226*, in press.
- Lin, R.P.: 2005, 'The Living With a Star (LWS) sentinels mission', *In SPIE Proc.*, **5901**, in press.
- Moses, J.D.: 2004, 'A private communication'.
- Newmark, J.: 2005, 'A private communication'.
- Tsurutani, B.T., Wu, S.T., Zhang, T.X., and Dryer, M.: 2003, 'Coronal Mass Ejection (CME)-induced shock formation, propagation and some temporally and spatially developing shock parameters relevant to particle energization', *Astron. and Astrophys.*, **412**, p. 293.
- Tsurutani, B.T., Judge, D.L., Guarneri, F.L., Gangopadhyay, P., Jones, A.R., Nuttall, J., Zambon, G.A., Didkovsky, L., Manuzzi, A.J., Iijima, B., Meier, R.R., Immel, T.J., Woods, T.N., Prasad, S., Huba, J., Solomon, S.C., Straus, P., Viereck, R.: 2005, 'The October 28, 2003 Extreme EUV Solar Flare and Resultant Extreme Ionospheric Effects: Comparison to Other Haloween Events and the Bastille Day Event', *GRL* **32**, L03S09.
- Williams, D.J., Arens, J.R. and Lanzerotti, L.J.: 1968, 'Observations of Trapped Electrons at Low and High Altitudes', *J. Geophys. Res.* **73**, p. 5673.

Ziegler, J.F., and Biersack, J.P.: 2003, 'The Stopping and Range of Ions in Matter (SRIM)', www.SRIM.com